HHS Public Access

Author manuscript

Neuron. Author manuscript; available in PMC 2020 August 07.

Published in final edited form as:

Neuron. 2019 August 07; 103(3): 459–472.e4. doi:10.1016/j.neuron.2019.05.025.

A specialized neural circuit gates social vocalizations in the mouse

Katherine Tschida[1], **Valerie Michael**[1], **Jun Takato**[1], **Bao-Xia Han**[1], **Shengli Zhao**[1], **Katsuyasu Sakurai**[1], **Richard Mooney**[1,2,3], **Fan Wang**[1,2]

[1]Department of Neurobiology, Duke University Medical Center, Durham, NC 27710, USA

[2]Senior Authors

[3]Lead contact

Summary

Vocalizations are fundamental to mammalian communication, but the underlying neural circuits await detailed characterization. Here we used an intersectional genetic method to label and manipulate neurons in the midbrain periaqueductal gray (PAG) that are transiently active in male mice when they produce ultrasonic courtship vocalizations (USVs). Genetic silencing of PAG-USV neurons rendered males unable to produce USVs and impaired their ability to attract females. Conversely, activating PAG-USV neurons selectively triggered USV production, even in the absence of any female cues. Optogenetic stimulation combined with axonal tracing indicate that PAG-USV neurons gate downstream vocal patterning circuits. Indeed, activating PAG neurons that innervate the nucleus retroambiguus, but not those innervating the parabrachial nucleus, elicited USVs in both male and female mice. These experiments establish that a dedicated population of PAG neurons gives rise to a descending circuit necessary and sufficient for USV production, while also demonstrating the communicative salience of male USVs.

Graphical Abstract

Correspondence: mooney@neuro.duke.edu.

Author contributions: RM, FW, and KT designed the experiments. KT, VM, and JT conducted the experiments. SZ made viruses. KS provided guidance in the use of the CANE method and made viruses. BXH provided animal husbandry and experimental support. RM, FW, and KT wrote the manuscript, and all authors approved the final manuscript.

Competing interests: The authors declare no competing interests.

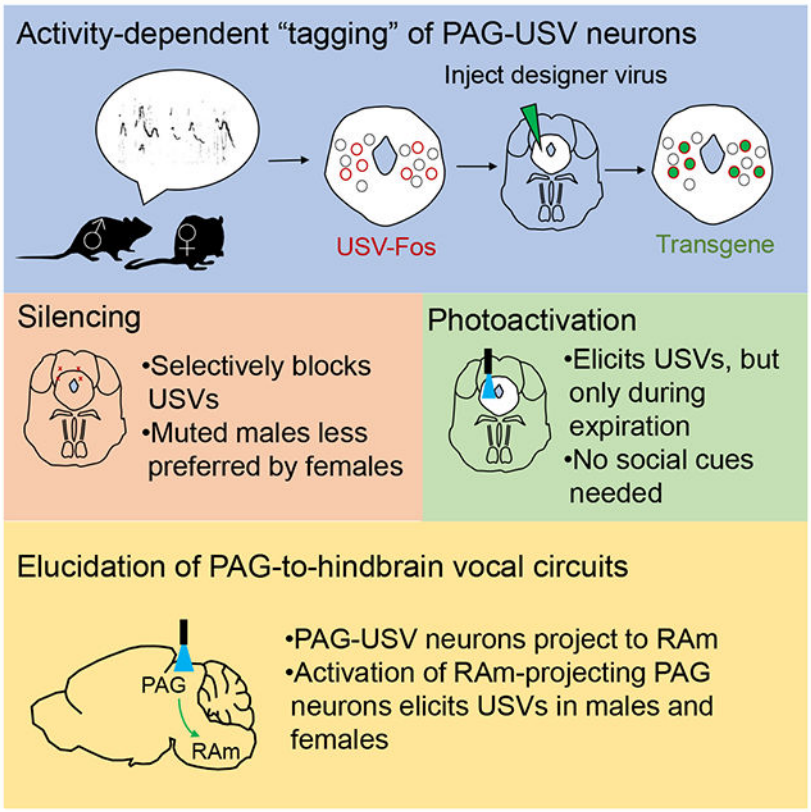

eTOC Blurb

Tschida et al. use an intersectional method to identify specialized midbrain neurons whose activity is necessary and sufficient for the production of social vocalizations in the mouse, affording an entry point for genetically dissecting the brain-wide circuits for vocal communication.

Keywords

vocalization; ultrasonic; periaqueductal gray; nucleus retroambiguus; activity-dependent labeling

Introduction

Vocalizations are an essential medium for communication in mammals ranging from mice to humans, conveying important information about the individual’s reproductive and social status, affective state, location, and identity, as well as the presence of food, kin, or predators. Vocalization requires coordinated phonation, articulation, and respiration and involves a neural network that spans the forebrain and brainstem (Jurgens, 2002, 2009; Simonyan, 2014). A key region in this network is the midbrain periaqueductal gray (PAG), which serves as an obligatory node for vocal control in primates, cats, and rodents (Jurgens, 2002, 2009). Indeed, bilateral lesions or inactivation of the PAG result in mutism (Adametz and O’Leary, 1959; Esposito et al., 1999; Jurgens, 1994, 2002, 2009; Jurgens and Pratt, 1979; Kittelberger et al., 2006; Skultety, 1962, 1965), while electrical or chemical activation

of the PAG can elicit vocalizations (Bandler and Carrive, 1988; Jurgens and Ploog, 1970; Kyuhou and Gemba, 1998; Lu and Jurgens, 1993; Magoun et al., 1937; Martin, 1976; Schuller and Radtke-Schuller, 1990; Suga et al., 1973; Waldbillig, 1975; Yajima et al., 1980; Zhang et al., 1994). Despite the PAG's importance for vocal production, the identity of the PAG neurons involved in vocalization has remained elusive.

A major challenge to identifying PAG neurons essential to vocalization is that the PAG is a functionally and anatomically heterogeneous structure that serves myriad roles including nociception, defensive behaviors, and autonomic regulation (Bandler and Shipley, 1994; Carrive, 1993; Evans et al., 2018; Holstege, 2014; Li et al., 2018; Tovote et al., 2016). Although chemical inactivation or electrical stimulation applied in the PAG can respectively suppress or trigger vocalizations, these gross manipulations also likely interfere with other non-vocal functions of PAG neurons. Consequently, whether the PAG contains a specific population of neurons dedicated to controlling vocalizations remains unclear. Furthermore, if such dedicated neurons exist, the ability to selectively excite or suppress them would greatly facilitate the systematic analysis of the communicative function of vocalizations. In fact, the inability to selectively manipulate vocalization-related PAG neurons has made it difficult to test an influential model in which the PAG gates downstream vocal-respiratory pattern generators, rather than serving as a component of this pattern generating network (Jurgens, 1994, 2002, 2009). Although the PAG sends descending projections to a variety of brainstem regions implicated in vocal-respiratory pattern generation (Cameron et al., 1995; Mantyh, 1983; Meller and Dennis, 1991; Vanderhorst et al., 2000a), the connectivity of vocalization-related PAG neurons remains unknown. Accordingly, the ability to selectively label vocalization-related PAG neurons is essential to map their connectivity with other brainstem regions and to test the functional contributions that these projections make to vocalization.

Overcoming these challenges requires novel genetic methods to selectively tag vocalization-related PAG neurons, map their connectivity, manipulate their activity, and test their relevance to vocal patterning and communication. The genetic methods necessary to such an endeavor are most practical in the mouse, which emits a rich repertoire of ultrasonic vocalizations (USVs) in a variety of social contexts, including during courtship (Holy and Guo, 2005; Maggio and Whitney, 1985; Neunuebel et al., 2015; Nyby et al., 1979; Portfors and Perkel, 2014; Whitney et al., 1974). Here we used an intersectional genetic "tagging" method (Rodriguez et al., 2017; Sakurai et al., 2016) to identify a distinct subset of PAG neurons in the male mouse that are selectively activated during USV production elicited by female cues. This approach allowed us to identify a specialized population of PAG neurons that are required for USV production, test the communicative salience of male USVs in promoting female social affiliation, and map a broader PAG-to-hindbrain circuit whose activation gates USV production in both male and female mice.

Results

The caudolateral PAG contains neurons that are active during USV production

Our overarching strategy was to use CANE, a recently developed intersectional genetic method that depends on the activity-dependent neural expression of the immediate early gene *c-Fos,* to identify and characterize vocalization-related PAG neurons in the mouse

(Rodriguez et al., 2017; Sakurai et al., 2016). Therefore, we first determined whether the PAG contains neurons that express Fos in a vocalization-contingent manner. We focused our attention on male courtship USVs, which comprise individual vocal elements (i.e., syllables) that are organized into multisyllabic bouts that last from hundreds of milliseconds to many seconds (Gourbal et al., 2004; Holy and Guo, 2005; Nyby, 1983; Nyby et al., 1979; White et al., 1998; Whitney et al., 1974) (Fig. 1A). Briefly, USVs were elicited from single-housed male mice by giving them a brief (~30 min) social experience with a female or by presenting them with female urine (Fig. 1A–B). These males were sacrificed ~2 hours from the start of the behavioral session and the expression of Fos protein was quantified throughout the PAG using immunohistochemical methods (Fig. 1C–D, see Methods). Notably, Fos expression was elevated in the caudolateral PAG in males that vocalized in response to females or female urine (Fig. 1C), but not in the PAG of males that failed to vocalize in response to females or female urine (Fig. 1C) or that were exposed to other non-social odors (data not shown). Across all mice, the number of Fos-positive neurons in the caudolateral PAG correlated positively and significantly with the number of USVs that the male produced (Fig. 1D; N = 12, female social partner; N = 10, female urine; N = 2, ethanol). We also observed increased Fos expression in the caudolateral PAG of mouse pups that were isolated from the nest and produced USVs, but not in those that were not isolated and did not produce USVs (Fig. S1). Here we refer to the subset of PAG neurons that display increased Fos expression during USV production as PAG-USV neurons. Although adult female mice sometimes produced USVs toward novel females, the degree to which a given female vocalized was in general less robust than courtship USVs produced by males (data not shown), and precise viral injections are not feasible in mouse pups. Thus, we restricted subsequent CANE-based experiments to adult male mice.

We performed two-color *in situ* hybridization to determine the neurotransmitter phenotype of PAG-USV neurons. In particular, we examined the expression of markers for glutamatergic (vesicular glutamate transporter 2, vGluT2) and GABAergic neurons (glutamic acid decarboxylase 1 and 2, GAD1 and GAD2) (Fig. 1E, see Methods). This analysis revealed that most PAG-USV neurons were glutamatergic (~75%, Fig. 1E left, red), and a minority were GABAergic (~25%, Fig. 1E right, red). In summary, the caudolateral PAG of the mouse contains a subset of mainly glutamatergic neurons that are activated during USV production.

Genetic tagging of PAG-USV neurons

Having identified a population of PAG neurons that exhibit USV-dependent expression of Fos, we used CANE (Rodriguez et al., 2017; Sakurai et al., 2016) to genetically label, identify, and manipulate PAG neurons that are selectively active when male mice produce courtship USVs (Fig. 2A). Briefly, the CANE method relies on: (1) a knock-in mouse in which expression of a destabilized TVA receptor (dsTVA) is driven by activation of the Fos promotor and hence is expressed in a similar spatial and temporal pattern as that of Fos (i.e., the Fos^{TVA} mouse); (2) a pseudotyped virus with a mutated envelope-A protein coat that can carry desired transgenes and can only infect neurons expressing the dsTVA receptor (a lentivirus driving Cre expression, CANE-LV-Cre).

We first used CANE to express GFP in PAG-USV neurons, allowing us to permanently label them, map their axonal projections, and establish whether they represent a stable neuronal population (Fig. 2B–D, and see below). Briefly, we elicited USVs from single-housed male Fos^{TVA} mice (~30 min session with female), then injected the caudolateral PAG with a combination of CANE-LV-Cre and AAV-FLEX-GFP viruses (Fig. 2A–C). This approach extensively labeled PAG-USV neurons with GFP (Fig. 2C), revealing that their axons terminate in a variety of targets in the midbrain, pons, and medulla (described in more detail below). We also established that almost half (46.0 ± 2.1%, N = 11 mice) of PAG neurons labeled with GFP following an encounter in which the male emitted USVs toward a female were re-activated (i.e., upregulated Fos) following a second round of USV production ~4 weeks later (Fig. 2C–D). This proportion of reactivated cells is ~ 50% greater than the number of double-labeled PAG neurons observed when the first vocal social encounter was followed 4 weeks later by a 30–60 minute period of wheel-running in the mouse's home cage (Fig. 1D, 29.9 ± 2.9%, N = 8, $p < 0.001$, Mann Whitney U test). We note that this degree of reactivation is comparable to what has been observed in previous studies using CANE and other Fos-based genetic labeling methods in other brain regions (DeNardo et al., 2019; Guenthner et al., 2013; Okuyama et al., 2016; Rodriguez et al., 2017). Therefore, many of the same PAG-USV neurons are active during vocal bouts separated by many weeks, indicating that a stable and distinct subpopulation of PAG neurons is activated during USV production.

Silencing PAG-USV neurons blocks USV production

To test whether the activity of PAG-USV neurons is causally linked to USV production, we used CANE to express tetanus toxin light chain (TeLC) in PAG-USV neurons, which over days to weeks irreversibly blocks their ability to release neurotransmitters (see Methods; CANE-LV-Cre and AAV-FLEX-TeLC injected bilaterally into the caudolateral PAG of a Fos^{TVA} male that had recently vocalized, Fig 2E). Blocking transmitter release from PAG-USV neurons strongly suppressed male USV production to nearby females: most (8/12) males were rendered completely mute for USV production, while the remaining 4 males emitted extremely low levels of USVs, and the extent of this vocal suppression was well related to the number of TeLC-expressing PAG-USV neurons (Fig. S2; 2 weeks after injection, mean USV counts were 4.7 ± 2.3% of pre-injection level; mean number of infected cells was 289 ± 88; Movies S1–2).

Although these findings are consistent with the idea that PAG-USV neurons are directly involved in USV production, silencing PAG-USV neurons could indirectly block vocalization, perhaps by decreasing social or sexual motivation. To control for this possibility, we compared the amount of time PAG_{USV}-TeLC males spent courting a female before and 2 weeks after viral injection (Fig. 2G). Although the mean amount of time spent engaged in courtship tended to decrease slightly post-injection (to 83.1 ± 16.5% pre-injection level, see Fig. S2 for low vs. high intensity courtship), this decrease was not significant (Fig. 2G, Fig. S2) and was not different from the change seen over 2 weeks in PAG_{USV}-GFP control males (81.8 ± 6.3% pre-injection courtship level, N = 14 mice). Therefore, in adult male mice encountering adult females, PAG-USV neurons are necessary for USV production but not for other (non-vocal) courtship behaviors.

Male courtship USVs promote female social affiliation

Male USVs are thought to act as courtship signals to elicit female approach (Egnor and Seagraves, 2016; Hammerschmidt et al., 2009; Pomerantz et al., 1983; Portfors and Perkel, 2014). However, because males normally produce USVs in concert with non-vocal courtship behaviors (Matsumoto and Okanoya, 2016; Neunuebel et al., 2015; Nyby, 1983; White et al., 1998), whether male USVs promote female social affiliation independently of these other courtship behaviors remains unclear. To begin to address this issue, we tested the preference of female mice for muted (TeLC-expressing) males versus control (GFP-expressing) males in a three-chambered preference test, during which the control male could freely vocalize, but neither male could engage in non-vocal courtship behaviors (Fig. 2H). On average, females tended to prefer vocalizing (GFP control) males over muted TeLC-expressing males ($p = 0.14$, Wilcoxon signed-rank test, $n = 37$ tests from pairs of males including $N = 5$ PAG_{USV} -TeLC and $N = 9$ PAG_{USV} -GFP males; females spent an average of 120 ± 8 s with PAG_{USV} -TeLC mice and 145 ± 9 s with PAG_{USV} -GFP males). If male USVs function to attract females, we hypothesized that the degree of female preference for control males should increase as a function of their vocal output. To test this idea, we ordered the trials according to the vocal output of the control male and then split the dataset in half (Fig. 2I). In support of our hypothesis, female preference was significantly biased toward GFP control males in trials in which these control males vocalized at high rates (mean female preference in high vocal rate trials was $0.60 +/- 0.04$, $p = 0.01$ for difference from mean = 0.5, single sample t-test). In contrast, females equally preferred GFP control and TeLC-expressing males when control males vocalized at low rates (mean preference score in low vocal rate trials was $0.48 +/- 0.05$, $p = 0.72$ for difference from mean = 0.5, single sample t-test). These findings show that high rates of male USVs can bias female social preference independently of other courtship behaviors, thus establishing a role for courtship USVs in promoting female social affiliation. These findings confirm and extend prior studies that induced male muting by laryngeal nerve cut (Pomerantz et al., 1983), which may impair other physiological aspects of male courtship performance, or that employed USV playback (Hammerschmidt et al., 2009; Willadsen et al., 2014; Wohr and Schwarting, 2007), which lacks other social cues that may be generated by a male social partner.

Activating PAG-USV neurons is sufficient to elicit USVs in the absence of social cues

If PAG-USV neuron activity is causally linked to vocalization, then activating these neurons may be sufficient to elicit USV production in the absence of any social cues. To test this idea, we used CANE to bilaterally express the excitatory DREADDs receptor hM3Dq in PAG-USV neurons (Fig. 3A). Six weeks later, we administered either CNO or saline (i.p.) and measured the vocal output of individual males while they were alone in a novel test chamber, a condition in which males normally emit few USVs (Fig. 3A, 9.3 ± 7.4 USVs over 60 min., $N = 4$). After CNO treatment, almost all (7/8) hM3Dq-expressing males dramatically increased their USV production (Fig. 3A; 279.4 ± 138.6 USVs over 60 min., $p = 0.02$, Wilcoxon signed-rank test, average number of infected neurons was $218 +/- 41$, see Fig. S3 for representative labeling). In contrast, the same mice treated with saline emitted USVs at low rates similar to socially isolated control males and to CNO-treated males that did not express the hM3Dq receptor (Fig. 3A, saline day: 17.0 ± 7.0 USVs, CNO only

males: 1.5 ± 0.9 USVs over 60 min., N = 4 mice). Thus, chemogenetic activation of PAG-USV neurons is sufficient to promote USV production in the absence of a female or female social cues.

To examine the linkage between PAG-USV neuronal activity and USV production with greater temporal precision, we used CANE to express channelrhodopsin (ChR2) in PAG-USV neurons and implanted fiber optics bilaterally over the caudolateral PAG. Optogenetically activating PAG-USV neurons with blue light was sufficient to rapidly and reliably elicit USVs in isolated males, indicating that activation of PAG-USV neurons is tightly coupled to USV production (Fig. 3B, and see also Fig. 4, trains: 5-10 Hz, 1-2s duration, USVs elicited in 73/82 trials; tonic pulses: 0.5-2s duration, USVs elicited in 28/30 trials; min. latency from laser onset to first USV was 23.4 ± 8.6 ms, mean latency was 406.6 ± 0.5 ms, n = 104 laser stimuli from N = 2 PAG_{USV}-ChR2 mice). The acoustic features of optogenetically-elicited USVs were largely similar to natural courtship USVs recorded from the same males, with subtle changes to certain acoustic parameters that fell within the normal range seen for courtship USVs; chemogenetically-elicited USVs also resembled natural courtship USVs but had more notable acoustic differences (Fig. 3B–C and Fig. S3). These findings show that activating a small (<500) and selective subset of PAG neurons is sufficient to elicit USVs in socially isolated male mice.

Electrical or chemical stimulation of the PAG elicits vocalization in a variety of mammals (Jurgens, 1994, 2002, 2009), but these vocalizations are often accompanied by additional defensive behaviors (Bandler and Carrive, 1988; Magoun et al., 1937; Waldbillig, 1975). Therefore, whether vocalization-related PAG neurons act as a discrete channel to selectively drive USV production or might also contribute to non-vocal motor behaviors remains unclear.

We first confirmed that in addition to enhancing USV production, non-selective chemogenetic or optogenetic activation of caudolateral PAG neurons drove pronounced locomotor effects, including freezing as well as ballistic, escape-like locomotor behaviors (Fig. S4, Movies S3–S4). In contrast, chemogenetic or optogenetic activation of CANE-tagged PAG-USV neurons elicited USVs without evoking any of these non-vocal behaviors (Fig. S4, Movies S5–6). These observations indicate that PAG-USV neurons are selectively involved in USV production and are intermingled with other neurons in the caudolateral PAG that contribute to various non-vocal behaviors (Bandler and Shipley, 1994; Carrive, 1993; Holstege, 2014; Tovote et al., 2016).

We note that although CANE-mediated optogenetic activation of PAG-USV neurons is capable of selectively driving USV production, the success rate of this experiment was low (optogenetically-elicited USVs were observed in 2 of 28 PAG_{USV}-ChR2 mice; neither USVs nor non-vocal movements were observed during laser stimulation in the other 26 animals). Three lines of evidence support the idea that the low success rate of this experiment is attributable to low viral efficiency. First, the two PAG_{USV}-ChR2 mice animals that emitted optogenetically-elicited USVs had among the highest numbers of neurons infected with the CANE-ChR2 viral strategy (Fig. S5; mean number of infected neurons was 392 ± 15 in these 2 mice). Second, using Fos expression as a surrogate for neuronal activation, we

confirmed that optogenetic stimulation activates PAG-USV neurons, even when it failed to elicit USVs (Fig. S5). Third, we performed additional experiments in which PAG-USV neurons were infected with pseudotyped lentiviruses that infect TVA-expressing neurons with greater efficiency but also with less selectivity than the CANE-LV-Cre virus (Sakurai et al., 2016; N = 3 mice injected with wild-type EnvA-LV-Cre, N=4 injected with mutated $EnvA^{M5}$-LV-Cre, see Methods). As expected, co-injection of these viruses with AAV-FLEX-ChR2 resulted in labeling of many more PAG neurons than obtained with the original CANE-ChR2 strategy (Fig. S5). Notably, this approach also yielded higher success rates of optogenetically-elicited USVs in the absence of any social cues (USVs in 2/4 $EnvA^{M5}$-injected mice and in 3/3 wild-type EnvA-injected mice), as well as optogenetic elicitation of non-vocal movements (observed in 4/4 $EnvA^{M5}$-injected mice and in 3/3 wild-type EnvA-injected mice). These results support the conclusion that the original CANE-ChR2 strategy affords us selective genetic access to PAG-USV neurons, albeit with a low success rate for optogenetic experiments.

PAG-USV neuronal activity gates USVs and specifies vocal bout duration

An influential idea is that neural activity in the PAG gates vocalization, rather than participating in the patterning of individual vocal elements (Jurgens, 1994, 2002, 2009). Here we tested this idea by comparing the temporal pattern of optogenetic stimulation of PAG-USV neurons to the temporal pattern of optogenetically-elicited USVs. Consistent with a vocal gating role for PAG-USV neurons, we found that the duration of a given vocal bout was positively correlated with the duration of the laser stimulus used to elicit vocalization (Fig. 4A, N = 6 PAG-ChR2 mice, N = 2 PAG_{USV}-ChR2 mice). We also observed that tonic (i.e., unpatterned) and 10 Hz laser stimuli both elicited bouts of multiple USV syllables (Fig. 3B, 4B) and that USV syllables elicited by tonic and 10Hz laser stimuli were of similar duration (Fig. 4C, 49.1 ± 27.3 ms for tonic, 45.3 ± 19.9 ms for 10 Hz, $p = 0.38$, Wilcoxon signed-rank test). Thus, sustained PAG-USV activation is required for sustained vocal output, but patterned PAG-USV activation is not necessary for the production of multi-syllabic vocal bouts.

These findings do not exclude the possibility that patterned PAG-USV activity, when present, is capable of driving the timing of individual USV syllables. To evaluate this possibility, we examined whether the onsets of USV syllables elicited by 10 Hz laser stimuli were entrained to the timing of the immediately preceding laser pulse. This analysis revealed that USV syllable onset times were not tightly entrained to a particular point in the laser duty cycle, indicating that the timing of PAG-USV activation does not precisely determine when USV syllables are initiated (Fig. 4D, E, left and middle panels, n = 645 USVs from PAG-ChR2 mice and n = 306 USVs from PAG_{USV}-ChR2 mice). Instead, USV syllable onsets were precisely aligned to the ongoing respiratory cycle, occurring just after the end of the inspiratory phase and during post-inspiration/expiration, as has been demonstrated in unrestrained, spontaneously vocalizing rodents (Alves et al., 2016; Sirotin et al., 2014) (Fig. 4D, E, right panel, n= 648 optogenetically-elicited USVs measured in a head-fixed PAG_{USV}-ChR2 mouse, see Methods). Accordingly, laser pulses that began during inspiration elicited USVs more effectively and more rapidly than laser pulses that began during expiration (Fig. 4F). We also found subtle effects of PAG-USV activation on respiration, including an

increase in the proportion of the respiratory cycle dedicated to post-inspiration/expiration (Fig. 4G–H, $p < 0.001$, Wilcoxon signed-rank test), consistent with observed changes in respiration that occur during USV production in freely behaving rodents (Sirotin et al., 2014). Taken together, these findings support the idea that elevated PAG-USV neural activity is required to initiate and sustain a vocal bout, while the onset of USV syllables within the bout is controlled largely by downstream vocal-respiratory pattern generating circuits.

PAG-USV neurons project to downstream vocal-respiratory centers

We used CANE to express GFP in PAG-USV neurons and map their axonal projections, allowing us to begin to determine how the PAG engages downstream circuits important to vocal-respiratory patterning (N = 4 mice, see Methods). We found that the axons of PAG-USV neurons terminate in pontine and medullary reticular regions that are speculated to contain vocal-respiratory pattern-generating circuits (Jurgens, 2002; Nunez-Abades et al., 1990; Van Daele and Cassell, 2009). These reticular targets of PAG-USV axons include the pontine reticular formation, the lateral parabrachial nucleus, the gigantocellular reticular formation of the rostral medulla, and the dorsal and ventral reticular formation of the caudal medulla, as well as to other regions of the brainstem reticular formation (Fig. 5). Conspicuously, we did not detect any GFP-labeled axons in nucleus ambiguus, which contains the laryngeal motor neurons, consistent with the idea that PAG-USV neurons are upstream of central pattern generating elements that directly engage the vocal motor neurons important to phonation. Indeed, in addition to their terminations in various reticular targets, axons of PAG-USV neurons terminate extensively in the nucleus retroambiguus (RAm), which contains premotor neurons that project to both laryngeal and expiratory motor neurons (Holstege, 1989; Jurgens, 2002; Vanderhorst et al., 2001; Vanderhorst et al., 2000b; Wild et al., 2009) (Fig. 5G). Notably, the production of male courtship USVs was also accompanied by high levels of Fos expression in RAm neurons, and this Fos expression was absent in muted mice in which PAG-USV neurons were silenced with TeLC (Fig. S2). Thus, PAG-USV neurons can excite downstream premotor neurons that are believed to be play a direct role in vocal-respiratory patterning.

Activating RAm-projecting PAG neurons elicits USVs in male and female mice

The current findings show that PAG-USV neurons project to numerous targets in the caudal brainstem, some of which also upregulate Fos during USV production (Fig. 5B–G, Fig. S6). However, an important remaining issue is to test whether these different projections are equally important for gating vocalization, or alternatively, whether PAG inputs to different downstream regions contribute differentially to vocal control. The dense axonal projections that PAG-USV neurons make to RAm and the pivotal location of RAm in the vocal-respiratory hierarchy suggest that the PAG-to-RAm projection is especially important to vocalization. Indeed, in cats, chemical activation of RAm can elicit acoustically abnormal vocalizations (Zhang et al., 1995; Zhang et al., 1992), and medullary lesions that include RAm abolish vocalizations elicited by electrical stimulation of the PAG (Shiba et al., 1997). These studies implicate RAm-projecting PAG neurons as important for vocal control, but the contribution of these neurons to vocalization remains to be directly tested in rodents as well as other mammals. To this end, we employed a dual viral strategy to selectively express ChR2 in PAG-RAm neurons (Fig. 6A) and optogenetically activated PAG-RAm neurons in

both male and female mice. In fact, unilateral optogenetic activation of PAG-RAm neurons was sufficient to elicit USV production in the absence of social cues in both males and females (N = 5 females, N = 4 males; Fig. 6B) and with acoustic features comparable to USVs produced spontaneously or evoked by optogenetic stimulation of CANE-tagged PAG-USV neurons (Fig. 6C, compare with Fig. 3C). Moreover, similar to USVs elicited by optogenetic activation of PAG-USV neurons, the duration of a given vocal bout was on average similar to the duration of the laser stimulus, although more and longer USVs were evoked by tonic rather than phasic (10 Hz) activation of RAm-projecting PAG neurons (Fig. S6). In contrast to the selective recruitment of vocalization elicited by CANE-based activation of PAG-USV neurons (Fig. 3 and Fig. S4), optogenetic activation of PAG-RAm neurons also elicited non-vocal motor behaviors such as locomotion and tail rattling (data not shown), as well as exerting effects on respiration (Fig. S6). Therefore, PAG-RAm neurons may comprise a heterogeneous population of cells, some that contribute to vocalization and others that contribute to non-vocal behaviors. In support of this idea, only about a fifth (22.7 +/− 3.9%, N = 5 mice) of PAG-RAm neurons increased Fos expression following USV production, compared to about half (46.0 ± 2.1%, N = 11 mice, as previously shown in Fig. 2D) of CANE-tagged PAG-USV neurons. In summary, activating PAG-RAm neurons robustly elicits USVs in both males and females, despite the fact that most of these cells do not exhibit vocalization-related increases in activity, underscoring the functional relevance of the PAG-to-RAm circuit for vocal gating.

A remaining possibility is that the activation of any downstream target of PAG-USV neurons is sufficient to gate USVs. To test this idea, we manipulated the activity of PAG neurons that project to the lateral parabrachial nucleus (PBn), a pontine region that is also innervated by PAG-USV neurons (Fig. 5D), upregulates Fos following USV production (Fig. S6), and that serves a role in vocal-respiratory coupling, locomotor-respiratory coupling, and more broadly in regulating expiratory duration (Dutschmann and Dick, 2012; Giraudin et al., 2012; Potts et al., 2005; Smotherman et al., 2006; Zuperku et al., 2017). However, optogenetically activating PAG-PBn neurons failed to elicit USV production (N = 3 mice) and instead elicited steady running (data not shown, observed in 2 of 3 mice) that was distinct from the ballistic, escape-like movements evoked by non-selective optogenetic activation of the PAG (see Fig. S4 and Movie S4). Thus, although PAG-USV neurons provide input to the PBn, the majority of PAG-PBn neurons apparently contribute mostly to non-vocal behaviors, as further evidenced by the small fraction of PAG-PBn neurons that upregulated Fos in association with USV production (8.7 +/− 0.4%, N = 2 mice).

Discussion

Here we used an intersectional, activity-dependent genetic strategy to identify neurons in the midbrain PAG whose activity is essential for the production of courtship USVs in the male mouse. Notably, silencing PAG-USV neurons selectively abolished USV production in male mice that were otherwise actively courting nearby females, while artificially activating these neurons was sufficient to drive vocalization in the absence of any social cues. Moreover, by selectively suppressing the male's ability to produce USVs while leaving his other courtship behaviors intact, we established a communicative function for male USVs in promoting female social affiliation. Optogenetic activation of PAG-USV neurons revealed that their

sustained activation is required for sustained vocal output, but that the pattern of elicited USVs is entrained to ongoing respiration and not to the pattern of PAG-USV activation. These findings are consistent with the idea that PAG-USV neurons excite downstream premotor vocal-respiratory neurons whose activity in turn determines the precise temporal and spectral features of vocal output. In support of this idea, anatomical mapping of the descending axonal projections of PAG-USV neurons revealed inputs to downstream vocal-respiratory regions, including a robust input to the premotor region RAm. Finally, we established that optogenetic activation of PAG neurons that project to RAm elicits USV production in both male and female mice, thus elucidating a midbrain-to-hindbrain circuit that plays an essential and privileged role in vocal gating in both sexes.

Although male courtship USVs are normally produced as part of a suite of sexual behaviors (Egnor and Seagraves, 2016; Matsumoto and Okanoya, 2016; Neunuebel et al., 2015; Nyby, 1983), we found that silencing PAG-USV neurons selectively abolished male USVs without decreasing non-vocal courtship behavior (Fig 2F–G). Likewise, selective chemogenetic and optogenetic activation of PAG-USV neurons elicited USV production without driving the production of associated courtship behaviors, such as increased locomotion (Fig. S4, Movies S5–6). Thus, the PAG contains a subset of neurons that are selectively involved in the production of USVs, adding to a growing body of evidence that the PAG and nearby regions contain anatomically distinct subsets of neurons specialized to drive specific behaviors important for reproduction, social affiliation, and active and passive defensive behaviors (Caggiano et al., 2018; Cho et al., 2017; Matthews et al., 2016; Tovote et al., 2016). Additionally, USV production can be elicited in both males and females, either by activation of PAG-RAm neurons (Fig. 6C) or by non-selective activation of PAG neurons (male data shown in Fig. S4; female data not shown), suggesting that the same population of PAG-USV neurons is essential for USV production in both sexes.

Selective and temporally precise optogenetic stimulation of PAG-USV neurons reveals that they gate rather than temporally pattern vocalization, providing strong experimental support for a longstanding model in which the PAG functions to engage downstream vocal-respiratory pattern generating circuitry without directly influencing vocal-respiratory patterning. Specifically, we found that optogenetically controlled PAG-USV neuronal activity initiates vocalization and determines the duration of vocal bouts but does not determine the precise timing of individual USV syllables. Instead, USVs elicited by optogenetic stimulation of PAG-USV neurons were entrained to ongoing respiration and not to the pattern of PAG-USV activation, with vocalizations occurring exclusively during post-inspiration. These findings support the idea that PAG-USV neurons function as an obligatory integrator where a variety of descending inputs conveying sensory and motivational signals converge to subsequently activate downstream vocal-respiratory premotor neurons.

The current study also provides insight into how PAG-USV neurons could access and influence the downstream vocal-respiratory network. Specifically, we found that PAG-USV axons terminate in the vocal-respiratory premotor region RAm and in other respiratory-related regions, including the PBn. We also noted that activating the PAG to RAm pathway was sufficient to elicit USVs, whereas activation of the PAG to PBn projection was not. Moreover, despite direct projections from PAG-USV neurons to various respiratory-related

premotor regions, stimulating PAG-USV neurons did not entrain or reset respiration, but instead elicited USV production in a manner that was subservient to the ongoing respiratory rhythm. Although how and where vocal commands from the PAG are integrated with the ongoing respiratory rhythm remains unknown, an intriguing possibility is that input from respiratory brainstem regions (Gerrits and Holstege, 1996; Song et al., 2012) could rhythmically gate the responsiveness of vocal premotor neurons, especially those in RAm, to PAG-USV input. One adaptive consequence of this arrangement is that the PAG can only excite vocal premotor neuron pools during the post-inspiratory phase of respiration, which along with the absence of a direct projection from PAG-USV neurons to the nucleus ambiguus, could ensure that the constriction of the vocal tract that enables vocal patterning does not interfere with inspiration. Regardless of exactly how PAG vocal commands are integrated with respiration, our finding that activation of PAG-RAm neurons is sufficient to elicit USV production advances this midbrain-to-hindbrain circuit as an important node for vocal control. Taken together, our findings establish that PAG-USV neurons provide an essential and selective pathway for vocal control in the mouse, affording an entry point for genetically dissecting the brain-wide circuits for vocal communication.

STAR Methods

CONTACT FOR REAGENT AND RESOURCE SHARING

Further information and requests for resources and reagents should be directed to the Lead Contact, Richard Mooney (mooney@neuro.duke.edu).

EXPERIMENTAL MODELS AND SUBJECT DETAILS

Animal statement.—All experiments were conducted according to protocols approved by the Duke University Institutional Animal Care and Use Committee.

Animals.—Adult (P60-90) male Fos^{TVA} mice (Jackson Laboratory, stock 027831) were used for capturing PAG-USV neurons with the CANE method (Rodriguez et al., 2017; Sakurai et al., 2016). Fos^{TVA} mice were housed on a reversed light/dark cycle and were single-housed beginning ~2-7 days prior to experimentation. Vglut2-ires-Cre (Jackson Laboratory, stock 028863) and PV-Cre (Jackson Laboratory stock 008069) group-housed adult males were used to express hM3Dq and ChR2 respectively in caudolateral PAG neurons.

METHOD DETAILS

USV recording and analysis.—To elicit USVs for subsequent Fos immunohistochemistry, single-housed males were presented with either a freely moving female, a female restrained in a small container that still permitted limited olfactory investigation by the male, or female urine (collected and pooled from multiple females immediately before test session, presented 2-4 times during a 60 min. session). To elicit USVs from mouse pups, an individual mouse pup was removed from the nest and placed in the recording chamber for 30 minutes, and then was placed under a heat lamp until sacrificed for subsequent Fos staining. USVs were recorded with an ultrasonic microphone (Avisoft, CMPA/CM16), amplified (Presonus TubePreV2), and digitized at 250 kHz (Spike

7, CED). USVs were detected using codes from the Holy lab (http://holylab.wustl.edu/) using the following parameters (mean frequency > 45 kHz; spectral purity > 0.3; spectral discontinuity < 0.85; min. USV duration = 5 ms; minimum inter-syllable interval = 30 ms). To elicit USVs for tagging of PAG-USV neurons using CANE, Fos^{TVA} males were given social experience with a female (30-60 min. session), either in their home cage fitted with an acoustically permeable lid or in a test chamber that had no lid and allowed easy microphone access. Sixty minutes from the start of the session, Fos^{TVA} males were anesthetized and taken for injection of the PAG with viruses (see below), such that injections began approximately 2 hours from the start of USV production. To elicit USVs from female mice, single-housed females were allowed to interact with a novel female during a 30-60 min. session.

Fos immunohistochemistry: Mice were deeply anaesthetized with isoflurane and then transcardially perfused with ice-cold 4% paraformaldehyde in 0.1 M phosphate buffer, pH 7.4 (4% PFA). Dissected brain samples were post-fixed overnight in 4% PFA at 4 °C, cryoprotected in a 30% sucrose solution in PBS at 4 °C for 48 hou rs, frozen in Tissue-Tek O.C.T. Compound (Sakura), and stored at −80 °C until sectioning. Brains were cut into 80 μm coronal sections, rinsed 3× in PBS, permeabilized for 3 hours in PBS containing 1% Triton X (PBST), and then blocked in 0.3% PBST containing 10% Blocking One (Nacalai Tesque; i.e., blocking solution). Sections were processed for 48 hours at 4 degrees with the primary antibody in blocking solution (1:400 goat anti-Fos, Santa Cruz, sc52-g), rinsed 3 × 10 mins. in PBS, then processed for 48 hours at 4 degrees with secondary antibodies in blocking solution (1:1000, Alexa Fluor 488 or 594 bovine anti-goat, Jackson Laboratories, plus 1:500 NeuroTrace, Invitrogen). Tissue sections rinsed again 3 × 10 mins. in PBS, mounted on slides, and coverslipped with Fluoromount-G (Southern Biotech). After drying, slides were imaged with a 10× objective on a Zeiss 700 laser scanning confocal microscope, and Fos-positive neurons within the PAG were counted manually. The boundaries of the PAG were defined in the following way for different planes of section: −3.88 mm caudal to bregma: Fos+ neurons were included from all of PAG, excluding the Edinger-Westphal nucleus; −4.2 mm caudal: all of the PAG, excluding the oculomotor nucleus and the supraoculomotor layers of the PAG; −4.4 and −4.6 mm caudal: all of the PAG, excluding the dorsal raphe; −4.8 and −5 mm caudal: all of the PAG dorsal to the ventral bound of the aqueduct.

Floating section two-color in situ hybridization: In situ hybridization was performed as previously described (Stanek et al., 2016) with each probe being applied to 60-μm thick coronal floating sections including the caudolateral PAG. GAD1, GAD2, and vGluT2 probes were created as previously described (Takatoh et al., 2013), and GAD1 and GAD2 probes were applied as a mixed probe. In situ hybridization for glutamatergic and GABAergic markers were performed on sections from different animals.

Viruses and expression of transgenes in PAG-USV neurons using the CANE method: To stably express transgenes in PAG-USV neurons, Fos^{TVA} males were given social experience with a female (30-60 mins.) that resulted in high levels of USV production (500-5000 USVs total). Males were then anesthetized (1.5-2% isoflurane), and the

caudolateral PAG was targeted for injection. The final injection coordinates were AP=−4.7 +/− 0.2 mm, ML= 0.7, DV= 1.75, and these were reached by making a small craniotomy at approximately AP=−3.3 +/− 0.2 mm, ML=0.7 and advancing the pipette back toward PAG at a 30 degree angle relative to vertical. The PAG was then injected with a mixture of CANE-LV-Cre and an AAV driving Cre-dependent expression of the transgene of interest (1:1 ratio, 400-500 nL total, pressure-injected with a Nanoject II (Drummond), 4.6 nL every 15s). CANE-LV-Cre, EnvA^{M5}-LV-Cre, and wild-type EnvA-LV-Cre were produced as previously described (Rodriguez et al., 2017; Sakurai et al., 2016). EnvA^{M5}-LV-Cre and EnvA-LV-Cre were co-injected with AAVs at a ratio of 4:1 (4 parts EnvA to 1 part AAV). The following AAVs were co-injected with CANE-LV-Cre: AAV2/1-CAG-FLEX-GFP (UNC Vector Core), AAV2/8-hSyn-FLEX-GFP (UNC Vector Core), AAV2/8-hSyn-FLEX-TeLC-P2A-GFP (produced as previously described (Zhang et al., 2015)), AAV-hSyn-FLEX-hM3Dq-mCherry (Addgene and also UNC Vector Core), and AAV2/1-CBA-FLEX-ChR2-mCherry (UPenn Vector Core). To non-selectively drive expression of ChR2 in caudolateral PAG neurons, PV-Cre males were injected unilaterally in the caudolateral PAG with AAV2/1-hSyn-ChR2-eYFP (UPenn Vector Core, 50 nL). To drive expression of hM3Dq in caudolateral PAG neurons, VGlut2-Cre males were injected unilaterally in the caudolateral PAG with AAV2/8-hSyn-FLEX-hM3Dq-mCherry (50 nL). The waiting times following virus injections were as follows: CANE-lenti-Cre plus AAV-FLEX-GFP, 4 weeks; CANE-lenti-Cre plus AAV-FLEX-TeLC, 2 weeks; CANE-lenti-Cre plus AAV-FLEX-hM3Dq, 6 weeks; CANE-lenti-Cre plus AAV-FLEX-ChR2, 4 weeks; AAV-ChR2 only, 3 weeks; AAV-FLEX-hM3Dq only, 6 weeks; LV-retro-Cre plus AAV-FLEX-ChR2, 3-4 weeks.

Estimation of efficiency of CANE-mediated labeling of PAG-USV neurons—We estimate that the total number of USV-Fos-positive neurons per mouse is approximately 2000 bilaterally (~1000 unilaterally). We arrived at this number by calculating the mean number of Fos-positive neurons in the PAG over the entire A/P range (−4.4 mm to −5 mm caudal to bregma) over which Fos expression was significantly related to total USVs (Fig. 1D) in males that vocalized to either a female social partner or to female urine. For the data shown in Fig. 2D, the total number of PAG-USV neurons labeled with GFP ranged from 80 to 640 (mean number is 212 +/− 48), and thus the total percentage of Fos-positive neurons that were tagged ranges from 8%-64% (average is 21% +/− 5%). We then divide these estimates by a factor of ~2, because the overlap of GFP-labeled neurons with subsequent USV-induced Fos was about half (46%, Fig. 2D), and we arrive at a final estimate that CANE-GFP labeling on average tags ~10% of the total population of PAG-USV neurons.

Viral labeling of PAG-RAm and PAG-PBn neurons: To selectively label PAG neurons that projected either to RAm or to the PBn, the caudolateral PAG was injected unilaterally with AAV2/1-hSyn-ChR2-eYFP (50 nl), and the downstream region (either PBn or RAm) was injected unilaterally with 150-250 nL of LV-retro-Cre. LV-retro-Cre was produced as previously described (Stanek et al., 2016; Zhang et al., 2015). An optogenetic ferrule was implanted over the PAG in the same surgery (see below), and viruses were allowed to express at least 3 weeks before testing the behavioral effects of optogenetic activation of these subsets of PAG neurons.

Quantification of courtship behavior: Time spent engaged in courtship behavior by either PAG_{USV}-TeLC males or control males was manually scored from videos recorded with a webcam (Logitech, 30 frames per second) in which the male was allowed to freely interact with a novel female placed in his home cage (30 min. session). Anogenital sniffing and following were scored as low intensity courtship behaviors, while mounting was scored as a high intensity courtship behavior.

Three-chambered social preference test: During an acclimation period, the female test mouse was placed in the central chamber and allowed to freely explore the three chambers for approximately 5 minutes. The female was then restricted within the central chamber, and a male was placed in each side chamber, restrained underneath a wire cage insert that permitted limited olfactory investigation of the female when she was nearby. The female was then allowed to move freely between the three chambers, and her preference for the PAG_{USV}-GFP control male was measured as (time spent on side with control male)/(time spent with control male + time spent with PAG_{USV}-TeLC male). An ultrasonic microphone was placed above each of the two side chambers, and we determined empirically that the USVs produced by the control PAG_{USV}-GFP could not be detected or appeared at much lower amplitude on the microphone on the opposite side of the chamber, thus allowing us to unambiguously assign all USVs as arising from the control male's side of the chamber. Although we cannot completely rule out the possibility that the female test mouse contributed a small amount to the total USV count, it has been reported that female mice vocalize to males when they are being actively courted and when the male is also vocalizing (Neunuebel et al., 2015). Even under these circumstances, females were reported to contribute ~20% of the total measured USVs (Neunuebel et al., 2015), and we never observed overlapping USVs that would indicate that the control male and the female were vocalizing at the same time. Female mice were of a variety of genotypes, always 2-3 months of age (to ensure that high frequency hearing was intact), and estrous state was not measured or controlled.

CNO dosage and delivery: PAG_{USV}-hM3Dq mice were lightly anesthetized with isoflurane and then injected i.p. with CNO (4 mg/kg from Sigma, or 15 mg/kg from Duke Small Molecule Synthesis Facility) or an equivalent volume of sterile saline. PAG-hM3Dq mice were injected with 1 mg/kg CNO (Duke Small Molecule Synthesis Facility) or an equivalent volume of sterile saline. CNO-only control mice were anesthetized lightly and injected i.p. with either 4 mg/kg CNO (Sigma) or 15 mg/kg CNO (Duke Small Molecule Synthesis Facility). PAG_{USV}-hM3Dq mice were tested first in the saline condition and then tested again 2-3 days later in the CNO condition.

Optogenetic stimulation of PAG neurons: Custom-made optogenetic ferrules were implanted bilaterally (PAG_{USV}-ChR2 mice, implanted 3-4 weeks following viral injection) or unilaterally (PAG-ChR2, PAG_{RAm}-ChR2, and PAG_{PBn}-ChR2 mice, implanted in the same surgery as viral injection) above the caudolateral PAG at least 1 week before the first optogenetic testing and were fixed to the skull using Metabond (Parkell). PAG neurons were optogenetically activated with illumination from a 473 nm laser (3-30 mW) at 5-10 Hz (50 ms pulses, 1-2s total) or with phasic laser pulses (0.05-2s duration). Laser power used was

2-3 mW for the non-selective optogenetic activation of PAG neurons, optogenetic activation of RAm-projecting PAG neurons, and optogenetic activation of PAG-USV neurons labeled using EnvA-LV-Cre or EnvA^{M5}-LV-Cre. For optogenetic activation of PAG-USV neurons labeled using CANE-LV-Cre, the laser power used was 25-30 mW. Laser powers were kept constant within a given experiment and were matched between 10 Hz and tonic stimuli for each animal. Laser stimuli were driven by computer-controlled voltage pulses (Spike 7, CED).

Quantification of optogenetically-elicited body movements: The mouse's position was measured using custom Matlab codes (K. Tschida) that detected and tracked the centroid of the mouse's body position across video frames (Logitech webcam, 30 frames per second), and speed of movement was calculated as the change in position across pairs of frames. To align movement with optogenetic activation of PAG neurons, we first estimated the temporal offset between the webcam video and USV audio by calculating the time of the peak cross-covariance between the high-pass filtered webcam audio and the low-pass filtered USV audio. This offset was then used to align the mouse's movement to the onset of each optogenetic laser stimulus.

Comparison of acoustic features of chemogenetically- and optogenetically-elicited USVs to female-directed USVs: We used custom Matlab codes to generate spectrograms of our audio recordings and manually annotated onset and offset times of all optogenetically-elicited USVs. For all annotated USVs, we calculated 5 acoustic features: (1) duration, (2) inter-syllable interval (defined as interval from start of one USV to start of the next USV, >1000 ms intervals not included in analysis), (3) mean pitch (dominant frequency calculated at each time point of the USV, then averaged across entire syllable), (4) pitch variance (defined as the variance of the dominant frequency for a syllable), and (5) amplitude (defined as bandpower from 30-125 kHz, converted to dB, and measured relative to quiet background noise in the recording). These measurements of acoustic features were compared to those taken from female-directed syllables produced by the same animals, as well as 15 control Fos^{TVA} males. Female-directed USVs were automatically detected using Matlab codes (http://holylab.wustl.edu/), but we also manually annotated and analyzed the acoustic features of a subset of female-directed USVs to ensure that any observed differences between conditions could not be attributed to the detection method.

Respiration measurements and analyses: An air flow sensor (Honeywell, AMW3300V) was placed as close as possible to the snout of a head-fixed PAG$_{USV}$-ChR2 male that was allowed to run on a treadmill. Custom Matlab codes (K. Tschida) were used to detect inspiration onset and expiration onset throughout the respiratory cycle. Briefly, breathing data were collected at 250 kHz (Spike 7, CED), downsampled to 1 kHz, and the portion of the breathing signal to be analyzed was detrended, mean-subtracted, and divided by its own standard deviation. The breathing signal was then inverted and converted into a binary vector (values>0 set to 1 and values<0 set to 0). Inspiration onset times were detected as signal crossings from 0 to 1, and inspiration offsets were detected as signal crossings from 1 to 0. Respiration rate over a given interval was calculated in Hz as 1/(mean time between inspiration onsets).

GFP labeling of PAG-USV neurons and axon projection tracing: PAG-USV neurons were labeled with GFP by injecting the caudolateral PAG of a Fos^{TVA} male with a mixture of CANE-lenti-Cre and AAV-FLEX-GFP following a vocal encounter with a female. After at least 4 weeks, PAG_{USV}-GFP males were sacrificed, their brains were processed as detailed above, and every other 80 micron-thick tissue section was imaged with a 10× objective on a Zeiss 700 laser scanning confocal microscope. To detect axons in each image, images were binarized using a custom Matlab code (J. Takatoh). Brain regions were then manually annotated (ImageJ), and the area in square pixels containing axons was calculated for each brain region for each mouse and then normalized by the area of that brain region. Brain regions with an innervation density of less than 0.07% or that were not observed to be innervated in 4/4 mice were excluded from analysis.

Data availability: The data that support the findings of this study are available from the corresponding author upon reasonable request.

Code availability: All custom-written Matlab codes used in this study are available from the corresponding author.

QUANTIFICATION AND STATISTICAL ANALYSES

Statistics: Non-parametric, two-sided statistical comparisons were used in all analyses (Mann Whitney to compare two groups of unpaired observations, Wilcoxon signed-rank for paired observations, alpha=0.05), with the exception of the comparison of time spent immobile for PAG-hM3Dq and PAG_{USV}-hM3Dq mice treated with saline and CNO (Fig. S4A), for which we used a two-way repeated measures ANOVA followed by post-hoc paired t-tests. No statistical methods were used to predetermine sample sizes. Error bars represent standard error of the mean unless otherwise noted.

Supplementary Material

Refer to Web version on PubMed Central for supplementary material.

Acknowledgements:

Thanks to Michael Booze for additional mouse husbandry. This work is supported by NIH grants MH103908 (to F.W), DC13826 (to R.M.) and MH117778 (to F.W. and R.M.).

References

Adametz J, and O'Leary JL (1959). Experimental mutism resulting from periaqueductal lesions in cats. Neurology 9, 636–642. [PubMed: 13791737]

Alves JA, Boerner BC, and Laplagne DA (2016). Flexible Coupling of Respiration and Vocalizations with Locomotion and Head Movements in the Freely Behaving Rat. Neural Plast 2016, 4065073. [PubMed: 27525126]

Atasoy D, Aponte Y, Su HH, and Sternson SM (2008). A FLEX switch targets Channelrhodopsin-2 to multiple cell types for imaging and long-range circuit mapping. J Neurosci 28, 7025–7030. [PubMed: 18614669]

Bandler R, and Carrive P (1988). Integrated defence reaction elicited by excitatory amino acid microinjection in the midbrain periaqueductal grey region of the unrestrained cat. Brain Res 439, 95–106. [PubMed: 3359200]

Bandler R, and Shipley MT (1994). Columnar organization in the midbrain periaqueductal gray: modules for emotional expression? Trends Neurosci 17, 379–389. [PubMed: 7817403]

Caggiano V, Leiras R, Goni-Erro H, Masini D, Bellardita C, Bouvier J, Caldeira V, Fisone G, and Kiehn O (2018). Midbrain circuits that set locomotor speed and gait selection. Nature 553, 455–460. [PubMed: 29342142]

Cameron AA, Khan IA, Westlund KN, and Willis WD (1995). The efferent projections of the periaqueductal gray in the rat: a Phaseolus vulgaris-leucoagglutinin study. II. Descending projections. J Comp Neurol 351, 585–601. [PubMed: 7721985]

Carrive P (1993). The periaqueductal gray and defensive behavior: functional representation and neuronal organization. Behav Brain Res 58, 27–47. [PubMed: 8136048]

Cho JR, Treweek JB, Robinson JE, Xiao C, Bremner LR, Greenbaum A, and Gradinaru V (2017). Dorsal Raphe Dopamine Neurons Modulate Arousal and Promote Wakefulness by Salient Stimuli. Neuron 94, 1205–1219 e1208. [PubMed: 28602690]

DeNardo LA, Liu CD, Allen WE, Adams EL, Friedmann D, Fu L, Guenthner CJ, Tessier-Lavigne M, and Luo L (2019). Temporal evolution of cortical ensembles promoting remote memory retrieval. Nat Neurosci 22, 460–469. [PubMed: 30692687]

Dutschmann M, and Dick TE (2012). Pontine mechanisms of respiratory control. Compr Physiol 2, 2443–2469. [PubMed: 23720253]

Egnor SR, and Seagraves KM (2016). The contribution of ultrasonic vocalizations to mouse courtship. Curr Opin Neurobiol 38, 1–5. [PubMed: 26789140]

Esposito A, Demeurisse G, Alberti B, and Fabbro F (1999). Complete mutism after midbrain periaqueductal gray lesion. Neuroreport 10, 681–685. [PubMed: 10208530]

Evans DA, Stempel AV, Vale R, Ruehle S, Lefler Y, and Branco T (2018). A synaptic threshold mechanism for computing escape decisions. Nature 558, 590–594. [PubMed: 29925954]

Gerrits PO, and Holstege G (1996). Pontine and medullary projections to the nucleus retroambiguus: a wheat germ agglutinin-horseradish peroxidase and autoradiographic tracing study in the cat. J Comp Neurol 373, 173–185. [PubMed: 8889920]

Giraudin A, Le Bon-Jego M, Cabirol MJ, Simmers J, and Morin D (2012). Spinal and pontine relay pathways mediating respiratory rhythm entrainment by limb proprioceptive inputs in the neonatal rat. J Neurosci 32, 11841–11853. [PubMed: 22915125]

Gourbal BE, Barthelemy M, Petit G, and Gabrion C (2004). Spectrographic analysis of the ultrasonic vocalisations of adult male and female BALB/c mice. Naturwissenschaften 91, 381–385. [PubMed: 15278217]

Guenthner CJ, Miyamichi K, Yang HH, Heller HC, and Luo L (2013). Permanent genetic access to transiently active neurons via TRAP: targeted recombination in active populations. Neuron 78, 773–784. [PubMed: 23764283]

Hammerschmidt K, Radyushkin K, Ehrenreich H, and Fischer J (2009). Female mice respond to male ultrasonic ‘songs’ with approach behaviour. Biol Lett 5, 589–592. [PubMed: 19515648]

Holstege G (1989). Anatomical study of the final common pathway for vocalization in the cat. J Comp Neurol 284, 242–252. [PubMed: 2754035]

Holstege G (2014). The periaqueductal gray controls brainstem emotional motor systems including respiration. Prog Brain Res 209, 379–405. [PubMed: 24746059]

Holy TE, and Guo Z (2005). Ultrasonic songs of male mice. PLoS Biol 3, e386. [PubMed: 16248680]

Jurgens U (1994). The role of the periaqueductal grey in vocal behaviour. Behav Brain Res 62, 107–117. [PubMed: 7945960]

Jurgens U (2002). Neural pathways underlying vocal control. Neurosci Biobehav Rev 26, 235–258. [PubMed: 11856561]

Jurgens U (2009). The neural control of vocalization in mammals: a review. J Voice 23, 1–10. [PubMed: 18207362]

Jurgens U, and Ploog D. (1970). Cerebral representation of vocalization in the squirrel monkey. Exp Brain Res 10, 532–554. [PubMed: 4988409]

Jurgens U, and Pratt R (1979). Role of the periaqueductal grey in vocal expression of emotion. Brain Res 167, 367–378. [PubMed: 109167]

Kittelberger JM, Land BR, and Bass AH (2006). Midbrain periaqueductal gray and vocal patterning in a teleost fish. J Neurophysiol 96, 71–85. [PubMed: 16598068]

Krashes MJ, Koda S, Ye C, Rogan SC, Adams AC, Cusher DS, Maratos-Flier E, Roth BL, and Lowell BB (2011). Rapid, reversible activation of AgRP neurons drives feeding behavior in mice. J Clin Invest 121, 1424–1428. [PubMed: 21364278]

Kyuhou S, and Gemba H (1998). Two vocalization-related subregions in the midbrain periaqueductal gray of the guinea pig. Neuroreport 9, 1607–1610. [PubMed: 9631474]

Li Y, Zeng J, Zhang J, Yue C, Zhong W, Liu Z, Feng Q, and Luo M (2018). Hypothalamic Circuits for Predation and Evasion. Neuron 97, 911–924 e915. [PubMed: 29398361]

Lu CL, and Jurgens U (1993). Effects of chemical stimulation in the periaqueductal gray on vocalization in the squirrel monkey. Brain Res Bull 32, 143–151. [PubMed: 8102315]

Maggio JC, and Whitney G (1985). Ultrasonic vocalizing by adult female mice (Mus musculus). J Comp Psychol 99, 420–436. [PubMed: 4075780]

Magoun HW, Atlas D, Ingersoll EH, and Ranson SW (1937). Associated Facial, Vocal and Respiratory Components of Emotional Expression: An Experimental Study. J Neurol Psychopathol 17, 241–255. [PubMed: 21623397]

Mantyh PW (1983). Connections of midbrain periaqueductal gray in the monkey. II. Descending efferent projections. J Neurophysiol 49, 582–594. [PubMed: 6300351]

Martin JR (1976). Motivated behaviors elicited from hypothalamus, midbrain, and pons of the guinea pig (Cavia porcellus). J Comp Physiol Psychol 90, 1011–1034. [PubMed: 1033210]

Matsumoto YK, and Okanoya K (2016). Phase-Specific Vocalizations of Male Mice at the Initial Encounter during the Courtship Sequence. PLoS One 11, e0147102. [PubMed: 26841117]

Matthews GA, Nieh EH, Vander Weele CM, Halbert SA, Pradhan RV, Yosafat AS, Glober GF, Izadmehr EM, Thomas RE, Lacy GD, et al. (2016). Dorsal Raphe Dopamine Neurons Represent the Experience of Social Isolation. Cell 164, 617–631. [PubMed: 26871628]

Meller ST, and Dennis BJ (1991). Efferent projections of the periaqueductal gray in the rabbit. Neuroscience 40, 191–216. [PubMed: 1646974]

Nelson A, Schneider DM, Takatoh J, Sakurai K, Wang F, and Mooney R (2013). A circuit for motor cortical modulation of auditory cortical activity. J Neurosci 33, 14342–14353. [PubMed: 24005287]

Neunuebel JP, Taylor AL, Arthur BJ, and Egnor SE (2015). Female mice ultrasonically interact with males during courtship displays. Elife 4.

Nunez-Abades PA, Portillo F, and Pasaro R (1990). Characterisation of afferent projections to the nucleus ambiguus of the rat by means of fluorescent double labelling. J Anat 172, 1–15. [PubMed: 2272895]

Nyby J (1983). Ultrasonic vocalizations during sex behavior of male house mice (Mus musculus): a description. Behav Neural Biol 39, 128–134. [PubMed: 6661142]

Nyby J, Wysocki CJ, Whitney G, Dizinno G, and Schneider J (1979). Elicitation of male mouse (Mus muscululs) ultrasonic vocalization: 1. Urinary Cues. Journal of Comparative and Physiological Psychology 93, 957–975.

Okuyama T, Kitamura T, Roy DS, Itohara S, and Tonegawa S (2016). Ventral CA1 neurons store social memory. Science 353, 1536–1541. [PubMed: 27708103]

Pomerantz SM, Nunez AA, and Bean NJ (1983). Female behavior is affected by male ultrasonic vocalizations in house mice. Physiol Behav 31, 91–96. [PubMed: 6685321]

Portfors CV, and Perkel DJ (2014). The role of ultrasonic vocalizations in mouse communication. Curr Opin Neurobiol 28, 115–120. [PubMed: 25062471]

Potts JT, Rybak IA, and Paton JF (2005). Respiratory rhythm entrainment by somatic afferent stimulation. J Neurosci 25, 1965–1978. [PubMed: 15728836]

Rodriguez E, Sakurai K, Xu J, Chen Y, Toda K, Zhao S, Han BX, Ryu D, Yin H, Liedtke W, et al. (2017). A craniofacial-specific monosynaptic circuit enables heightened affective pain. Nat Neurosci 20, 1734–1743. [PubMed: 29184209]

Sakurai K, Zhao S, Takatoh J, Rodriguez E, Lu J, Leavitt AD, Fu M, Han BX, and Wang F (2016). Capturing and Manipulating Activated Neuronal Ensembles with CANE Delineates a Hypothalamic Social-Fear Circuit. Neuron 92, 739–753. [PubMed: 27974160]

Schuller G, and Radtke-Schuller S (1990). Neural control of vocalization in bats: mapping of brainstem areas with electrical microstimulation eliciting species-specific echolocation calls in the rufous horseshoe bat. Exp Brain Res 79, 192–206. [PubMed: 2311697]

Shiba K, Umezaki T, Zheng Y, and Miller AD (1997). The nucleus retroambigualis controls laryngeal muscle activity during vocalization in the cat. Exp Brain Res 115, 513–519. [PubMed: 9262206]

Simonyan K (2014). The laryngeal motor cortex: its organization and connectivity. Curr Opin Neurobiol 28, 15–21. [PubMed: 24929930]

Sirotin YB, Costa ME, and Laplagne DA (2014). Rodent ultrasonic vocalizations are bound to active sniffing behavior. Front Behav Neurosci 8, 399. [PubMed: 25477796]

Skultety FM (1962). Experimental mutism in dogs. Arch Neurol 6, 235–241. [PubMed: 13913743]

Skultety FM (1965). Mutism in Cats with Rostral Midbrain Lesions. 1. Arch Neurol 12, 211–225. [PubMed: 14237779]

Smotherman M, Kobayasi K, Ma J, Zhang S, and Metzner W (2006). A mechanism for vocal-respiratory coupling in the mammalian parabrachial nucleus. J Neurosci 26, 4860–4869. [PubMed: 16672660]

Song G, Wang H, Xu H, and Poon CS (2012). Kolliker-Fuse neurons send collateral projections to multiple hypoxia-activated and nonactivated structures in rat brainstem and spinal cord. Brain Struct Funct 217, 835–858. [PubMed: 22286911]

Stanek E.t., Rodriguez E, Zhao S, Han BX, and Wang F (2016). Supratrigeminal Bilaterally Projecting Neurons Maintain Basal Tone and Enable Bilateral Phasic Activation of Jaw-Closing Muscles. J Neurosci 36, 7663–7675. [PubMed: 27445144]

Suga N, Schlegel P, Shimozawa T, and Simmons J (1973). Orientation sounds evoked from echolocating bats by electrical stimulation of the brain. J Acoust Soc Am 54, 793–797. [PubMed: 4754391]

Takatoh J, Nelson A, Zhou X, Bolton MM, Ehlers MD, Arenkiel BR, Mooney R, and Wang F (2013). New modules are added to vibrissal premotor circuitry with the emergence of exploratory whisking. Neuron 77, 346–360. [PubMed: 23352170]

Tovote P, Esposito MS, Botta P, Chaudun F, Fadok JP, Markovic M, Wolff SB, Ramakrishnan C, Fenno L, Deisseroth K, et al. (2016). Midbrain circuits for defensive behaviour. Nature 534, 206–212. [PubMed: 27279213]

Van Daele DJ, and Cassell MD (2009). Multiple forebrain systems converge on motor neurons innervating the thyroarytenoid muscle. Neuroscience 162, 501–524. [PubMed: 19426785]

Vanderhorst VG, Terasawa E, and Ralston HJ 3rd (2001). Monosynaptic projections from the nucleus retroambiguus region to laryngeal motoneurons in the rhesus monkey. Neuroscience 107, 117–125. [PubMed: 11744252]

Vanderhorst VG, Terasawa E, Ralston HJ 3rd, and Holstege G (2000a). Monosynaptic projections from the lateral periaqueductal gray to the nucleus retroambiguus in the rhesus monkey: implications for vocalization and reproductive behavior. J Comp Neurol 424, 251–268. [PubMed: 10906701]

Vanderhorst VG, Terasawa E, Ralston HJ 3rd, and Holstege G (2000b). Monosynaptic projections from the nucleus retroambiguus to motoneurons supplying the abdominal wall, axial, hindlimb, and pelvic floor muscles in the female rhesus monkey. J Comp Neurol 424, 233–250. [PubMed: 10906700]

Waldbillig RJ (1975). Attack, eating, drinking, and gnawing elicited by electrical stimulation of rat mesencephalon and pons. J Comp Physiol Psychol 89, 200–212. [PubMed: 1171125]

White NR, Prasad M, Barfield RJ, and Nyby JG (1998). 40- and 70-kHz vocalizations of mice (Mus musculus) during copulation. Physiol Behav 63, 467–473. [PubMed: 9523885]

Whitney G, Alpern M, Dizinno G, and Horowitz G (1974). Female odors evoke ultrasounds from male mice. Anim Learn Behav 2, 13–18. [PubMed: 4468889]

Wild JM, Kubke MF, and Mooney R (2009). Avian nucleus retroambigualis: cell types and projections to other respiratory-vocal nuclei in the brain of the zebra finch (Taeniopygia guttata). J Comp Neurol 512, 768–783. [PubMed: 19067354]

Willadsen M, Seffer D, Schwarting RK, and Wohr M (2014). Rodent ultrasonic communication: Male prosocial 50-kHz ultrasonic vocalizations elicit social approach behavior in female rats (Rattus norvegicus). J Comp Psychol 128, 56–64. [PubMed: 24188619]

Wohr M, and Schwarting RK (2007). Ultrasonic communication in rats: can playback of 50-kHz calls induce approach behavior? PLoS One 2, e1365. [PubMed: 18159248]

Yajima Y, Hayashi Y, and Yoshii N (1980). The midbrain central gray substance as a highly sensitive neural structure for the production of ultrasonic vocalization in the rat. Brain Res 198, 446–452. [PubMed: 7407609]

Zhang SP, Bandler R, and Davis PJ (1995). Brain stem integration of vocalization: role of the nucleus retroambigualis. J Neurophysiol 74, 2500–2512. [PubMed: 8747209]

Zhang SP, Davis PJ, Bandler R, and Carrive P (1994). Brain stem integration of vocalization: role of the midbrain periaqueductal gray. J Neurophysiol 72, 1337–1356. [PubMed: 7807216]

Zhang SP, Davis PJ, Carrive P, and Bandler R (1992). Vocalization and marked pressor effect evoked from the region of the nucleus retroambigualis in the caudal ventrolateral medulla of the cat. Neurosci Lett 140, 103–107. [PubMed: 1383887]

Zhang Y, Zhao S, Rodriguez E, Takatoh J, Han BX, Zhou X, and Wang F (2015). Identifying local and descending inputs for primary sensory neurons. J Clin Invest 125, 3782–3794. [PubMed: 26426077]

Zuperku EJ, Stucke AG, Hopp FA, and Stuth EA (2017). Characteristics of breathing rate control mediated by a subregion within the pontine parabrachial complex. J Neurophysiol 117, 1030–1042. [PubMed: 27974449]

Highlights

- Specialized midbrain neurons are active when mice produce courtship vocalizations
- Silencing these neurons blocks vocalization but does not impair non-vocal courtship
- Activating these neurons elicits vocalization, even in the absence of social cues
- Activation and tracing show that these neurons gate premotor patterning circuits

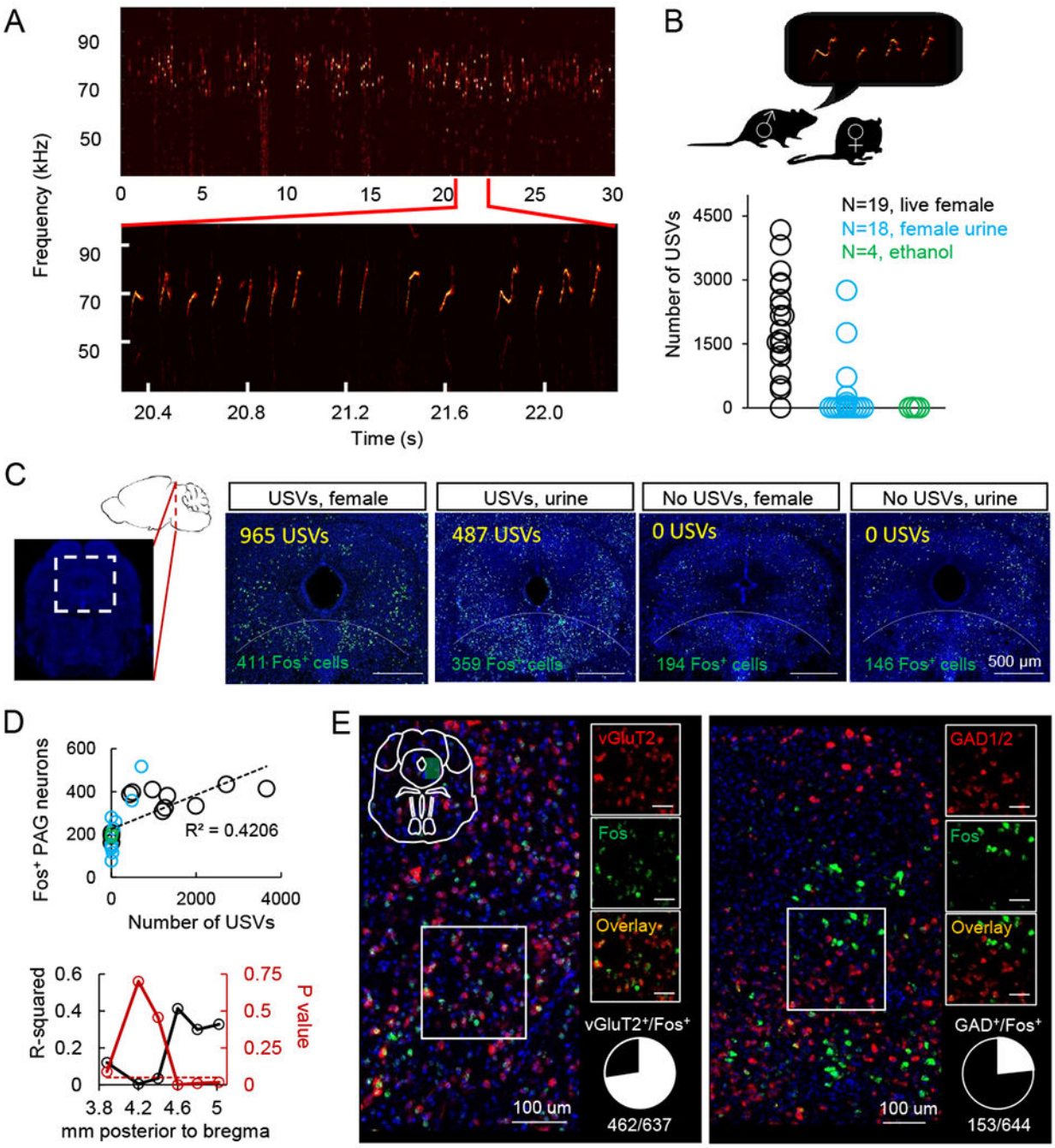

Figure 1. The caudolateral PAG contains neurons that are active during USV production.

(A) Spectrogram of USVs produced by a male mouse during a social encounter with a female. Inset shows expanded view. (B) Quantification of number of USVs produced by male mice during encounters with female social partners (black), female urine (blue), or a non-social odor, ethanol (green). (C) Left-most panel shows location of the caudolateral PAG in sagittal and coronal section. Four right-most panels show representative confocal images of Fos expression in the caudolateral PAG following social experience with a female social partner accompanied by USV production, female urine accompanied by USV

production, female social partner without USV production, and female urine without USV production (green, Fos; blue, NeuroTrace). Dotted line delineates the boundary dorsal to which PAG Fos+ neurons were quantified in this plane of section (see Methods). (D) (Top) The total number of Fos-positive caudolateral PAG neurons is positively correlated with the number of USVs produced by different males. Quantification is shown for the same plane of section as in (C), and color-coding is as in (B). (Bottom) The strength (R^2) and significance (p value) of the linear regression between the number of USVs produced and Fos expression in the caudolateral PAG is plotted across a 1.2 mm extent of the PAG (N = 12 males given female social partner; N = 10 female urine; N = 2 ethanol). (E) Two-color *in situ* hybridization, showing the overlap of caudolateral PAG neurons expressing *c-Fos* mRNA (green) following USV production and also either *vGluT2* (red, left) or *GAD1/2* (red, right) mRNA. Scale bars on insets, 50 um. See also Fig. S1.

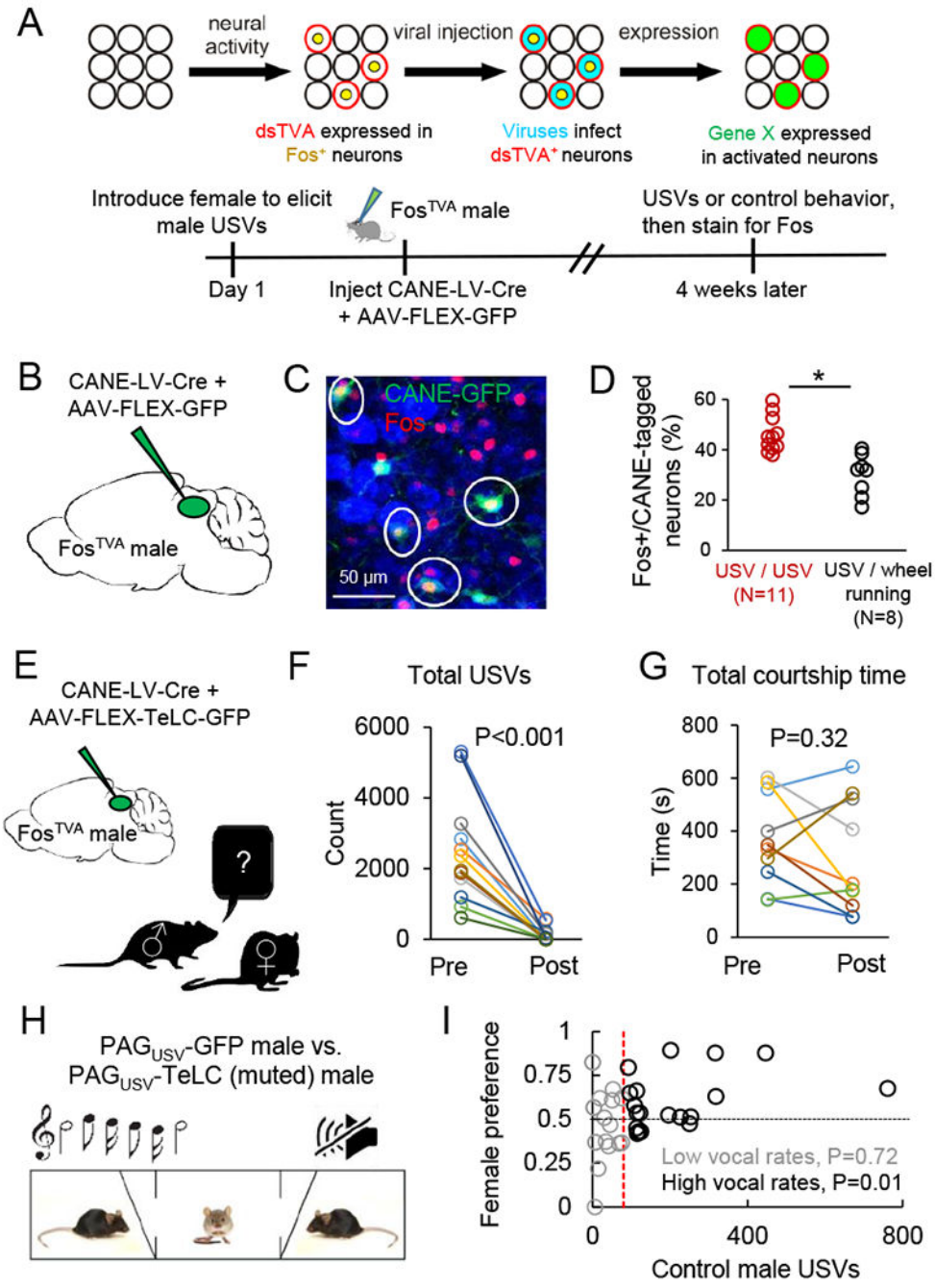

Figure 2. The production of courtship USVs requires PAG-USV neurons and promotes female social affiliation.

(A) Schematic of the CANE method (top) and the experimental time line to permanently express transgenes in PAG-USV neurons using CANE (bottom). (B) Schematic of the viruses injected into the caudolateral PAG of a Fos^{TVA} male following a vocal encounter with a female to label PAG-USV neurons with GFP. (C) Confocal image showing overlap between CANE-GFP-labeled PAG-USV neurons (green) after USV production toward a female and Fos (red) induced by a subsequent vocal encounter with a female. (D) Quantification of the overlap between CANE-GFP-labeled PAG-USV neurons and Fos

expression elicited by USVs (red points) or by wheel running in the home cage (black). (E) Schematic of the viruses injected into the caudolateral PAG of a Fos^{TVA} male to express tetanus toxin (TeLC) in PAG-USV neurons. (F) Blocking neurotransmitter release from PAG-USV neurons with CANE-driven expression of TeLC abolishes the production of male courtship USVs (N = 12 mice, $p < 0.001$, Wilcoxon signed-rank test). (G) Blocking neurotransmitter release from PAG-USV neurons has no significant effect on total time spent courting a female ($p = 0.32$, Wilcoxon signed-rank test). (H) Schematic of the three-chambered test. (I) Vocal output of the control PAG_{USV}-GFP male is plotted against female preference for that male (> 0.5 is preference for control male)). N = 37 tests from N = 5 PAG_{USV}-TeLC mice each paired against 1-3 PAG_{USV}-GFP controls, with each TeLC/GFP pair tested with 2-4 females. The red vertical line indicates where the dataset was split into low vocal rate trials (gray) and high vocal rate trials (black). See also Fig. S2.

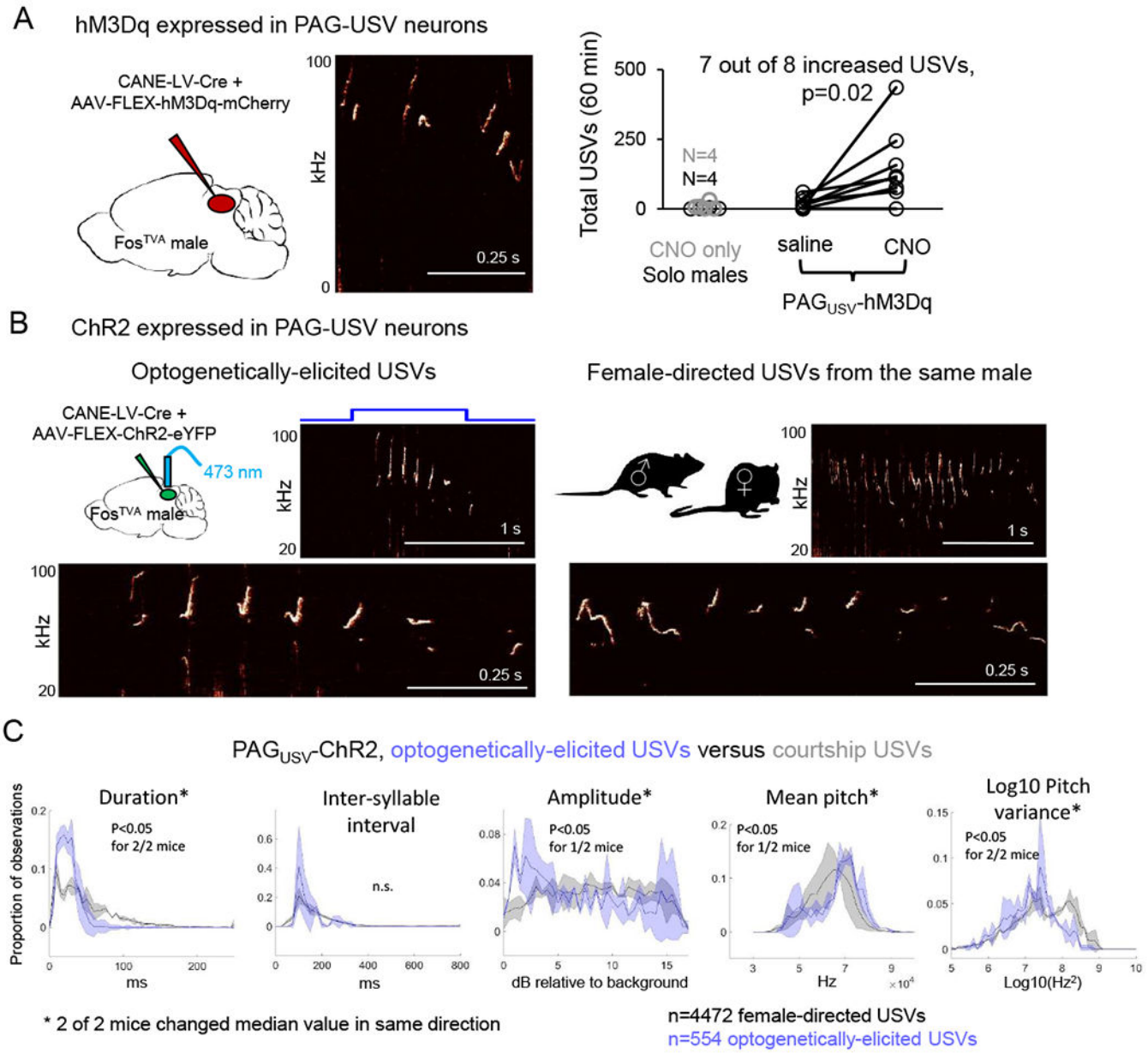

Figure 3. Activating PAG-USV neurons is sufficient to elicit USV production in the absence of social cues

(A) (Left) Schematic of the viruses injected into the caudolateral PAG of a Fos^{TVA} male to express hM3Dq in PAG-USV neurons. (Middle) Spectrogram showing USVs produced by a CNO-treated PAG_{USV}-hM3Dq male. (Right) Total USVs produced in a 60 min. solo test period are shown for different groups of males in chemogenetic experiments: control males (no virus, no CNO, black), males not expressing hM3Dq but treated with CNO (gray), and males with CANE-driven expression of hM3Dq in PAG-USV neurons that were treated with saline (i.p.) or CNO ($p = 0.02$ for PAG_{USV}-hM3Dq mice saline versus CNO USVs, Wilcoxon signed-rank test). (B) Optogenetic activation of PAG-USV neurons elicits USVs from males in the absence of female cues. Spectrograms comparing optogenetically-elicited

USVs (left) and female-directed USVs (right) from the same male. Bottom panels show expanded views. (C) Distributions of 5 acoustic parameters are shown for optogenetically-elicited USVs (blue) and female-directed USVs (gray) for 2 PAG_{USV}-ChR2 mice. Asterisks indicate acoustic parameters whose median value changed significantly in the same direction for both mice ($p < 0.05$, Mann Whitney U tests). See also Figs. S3–5.

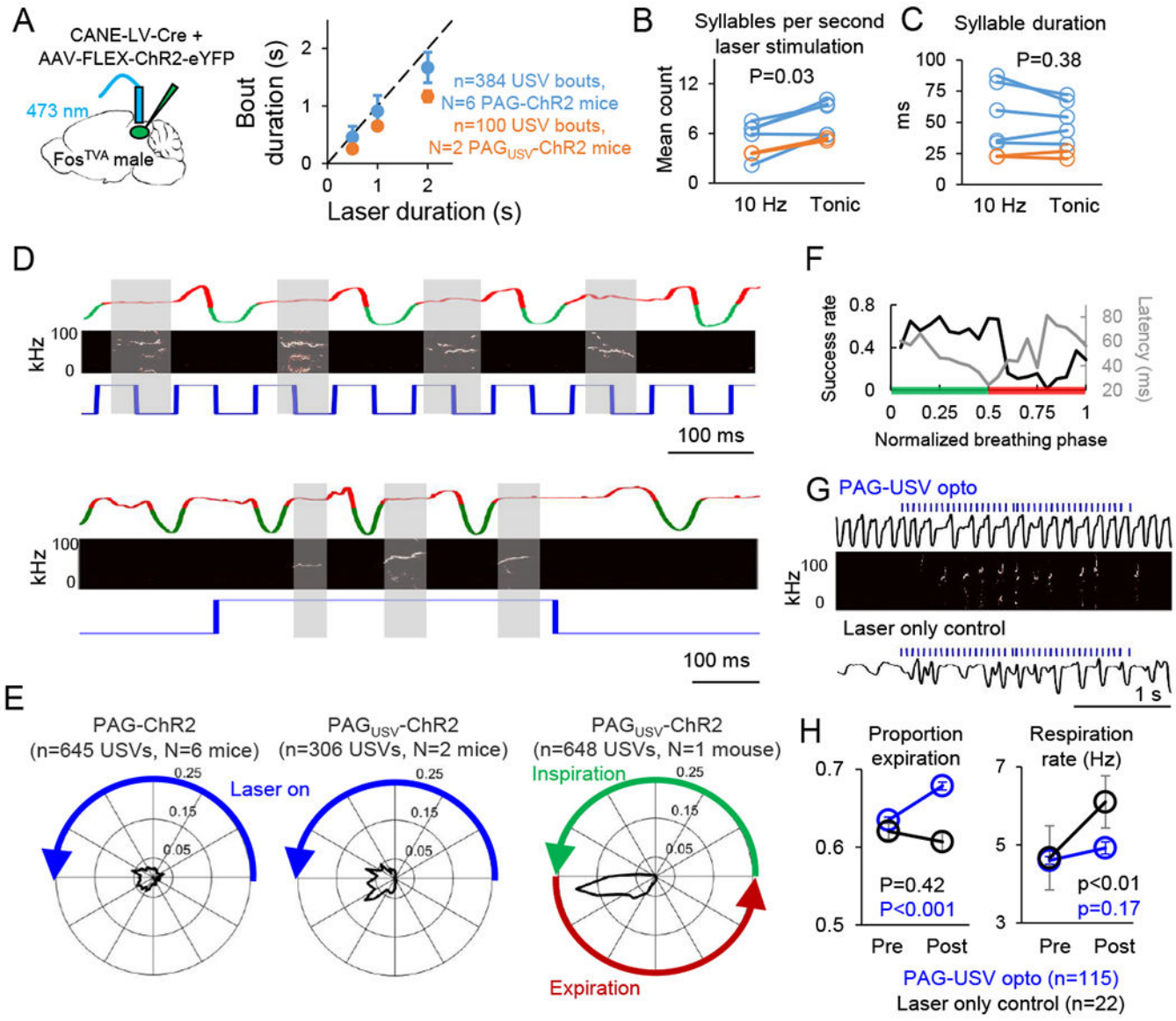

Figure 4. PAG-USV neuronal activity gates USVs and specifies vocal bout duration

(A) (Left) Schematic of the viruses injected into the caudolateral PAG of a Fos^{TVA} male to express ChR2 in PAG-USV neurons. (Right) The duration of optogenetically-elicited bouts of USVs is similar to the duration of laser stimuli used to activate PAG-USV neurons (mean ± SE).(B) Comparison of the number of USV syllables elicited per second of laser stimulation is shown for 10 Hz versus tonic laser stimuli for PAG-ChR2 mice (blue) and PAG_{USV}-ChR2 mice (orange; p = 0.03 for difference, Wilcoxon signed-rank test). (C) Same as (B), except comparing mean syllable duration for optogenetically-elicited USVs optogenetically (p = 0.38). (D) Representative portions of two bouts of optogenetically-elicited USVs are shown for a PAG_{USV}-ChR2 mouse, with breathing shown in the top traces (inspirations are downward deflections in green, expiration is shown in red, see Methods), USVs shown in the spectrograms (middle), and laser stimuli shown in blue (bottom). Gray shading shows the clear alignment between USVs and expiration. (E) (Left, middle) Polar

plots showing the distribution of onset times of individual optogenetically-elicited USV syllables relative to the duty cycle of the preceding laser pulse (10 Hz, 50ms on and 50ms off) for PAG-ChR2 mice (left) and PAG_{USV}-ChR2 mice (middle). Blue line indicates the laser-on portion of the laser duty cycle. Radial values (ranging from 0 to 0.25) represent proportion of total observations at a given time in the laser duty cycle, and total area inside the shaded black line is equal to one. (Right) Polar plot showing the distribution of onset times of individual optogenetically-elicited USV syllables relative to the respiratory cycle. (F) The probability of obtaining an optogenetically-elicited USV (black) and the mean latency from laser onset to USV onset (gray) are plotted in relation to the time that each laser pulse fell within the respiratory cycle (see Methods; green shading indicates inspiration, red shading indicates expiration, n = 1051 laser pulses from N = 1 PAG_{USV}-ChR2 mouse). (G) Breathing traces are shown for a PAG_{USV}-ChR2 mouse during optogenetic activation of PAG-USV neurons (top, breathing shown in black, laser in blue, USVs in spectrogram) and during a control period in which the laser was turned on but was disconnected from the optogenetic ferrule (bottom; breathing, black; laser, blue). (H) Optogenetic activation of PAG-USV neurons caused a significant increase in the proportion of the respiratory cycle occupied by expiration (left, blue, $p < 0.001$, Wilcoxon signed-rank test) and no change in respiration rate (right, blue). When the laser was not connected to the ferrule, laser light alone did not change the expiration/inspiration ratio (left, black, $p = 0.42$) and caused a significant increase in breathing rate (right, black, $p < 0.01$), likely due to a startle response (mean ± SE).

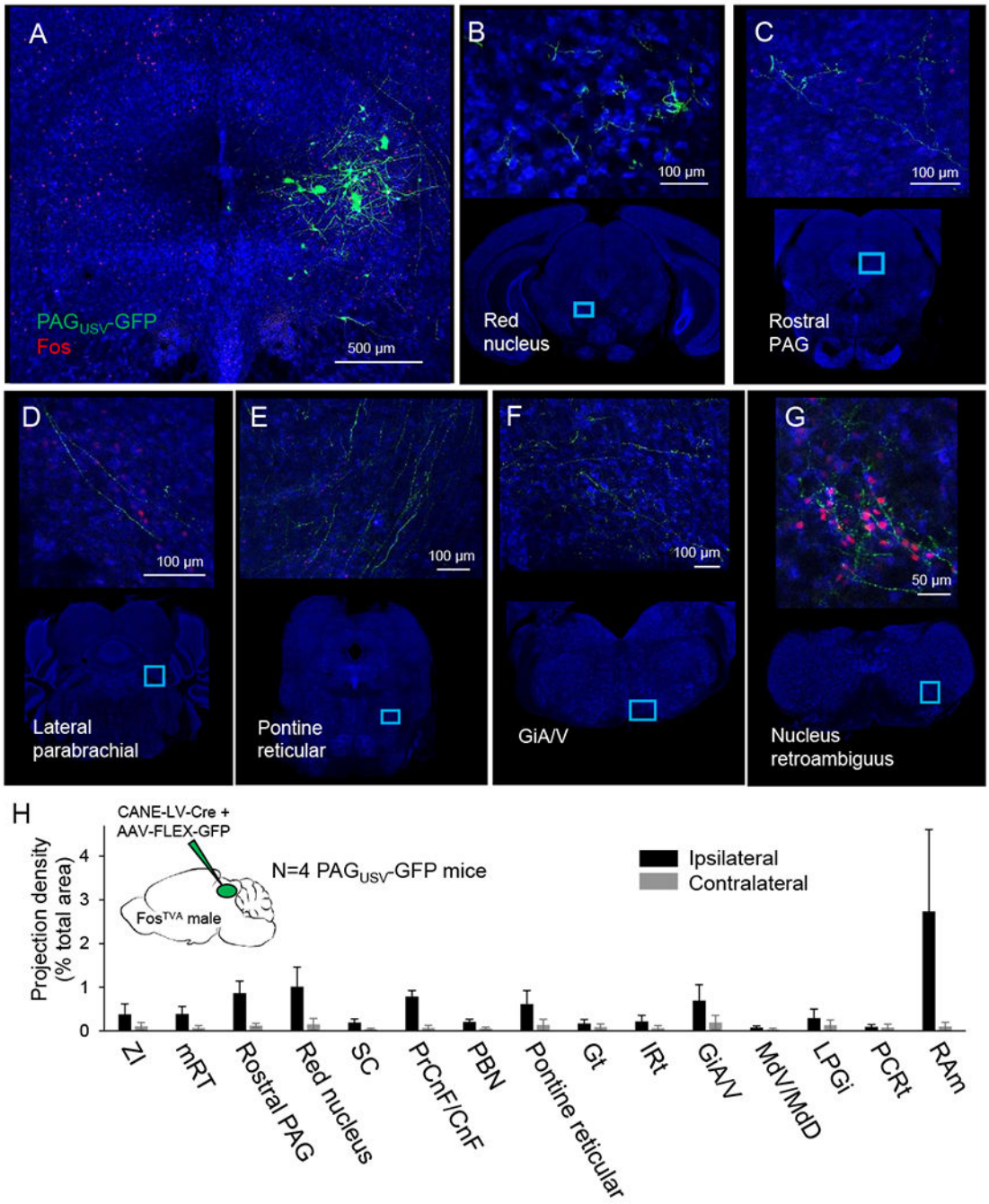

Figure 5. PAG-USV neurons project to downstream vocal-respiratory centers

Representative confocal images show (A) representative CANE-driven GFP labeling of PAG-USV cell bodies and PAG-USV axonal projections to (B) the red nucleus, (C) rostral PAG, (D) the lateral parabrachial nucleus, (E) the pontine reticular formation, (F) the magnocellular reticular formation of the rostral medulla, and (G) nucleus retroambiguus in the caudal medulla. (H) Quantification of axonal projections, presented as projection density (total square pixels of axonal innervation normalized by the total area of each region, organized rostral to caudal, see Methods, N = 4 mice, mean ± SE). ZI, zona incerta; mRT,

mesencephalic reticular formation; SC, superior colliculus; PrCnF, precuneiform; CnF, cuneiform; PBn, parabrachial nucleus; Gt, gigantocellular reticular formation; IRt, intermediate reticular formation; GiA/V, magnocellular reticular formation; MdV, ventral medullary reticular formation; MdD, dorsal medullary reticular formation; LPGi, paragigantocellular reticular formation; PCRt, parvocellular reticular formation; RAm, nucleus retroambiguus.

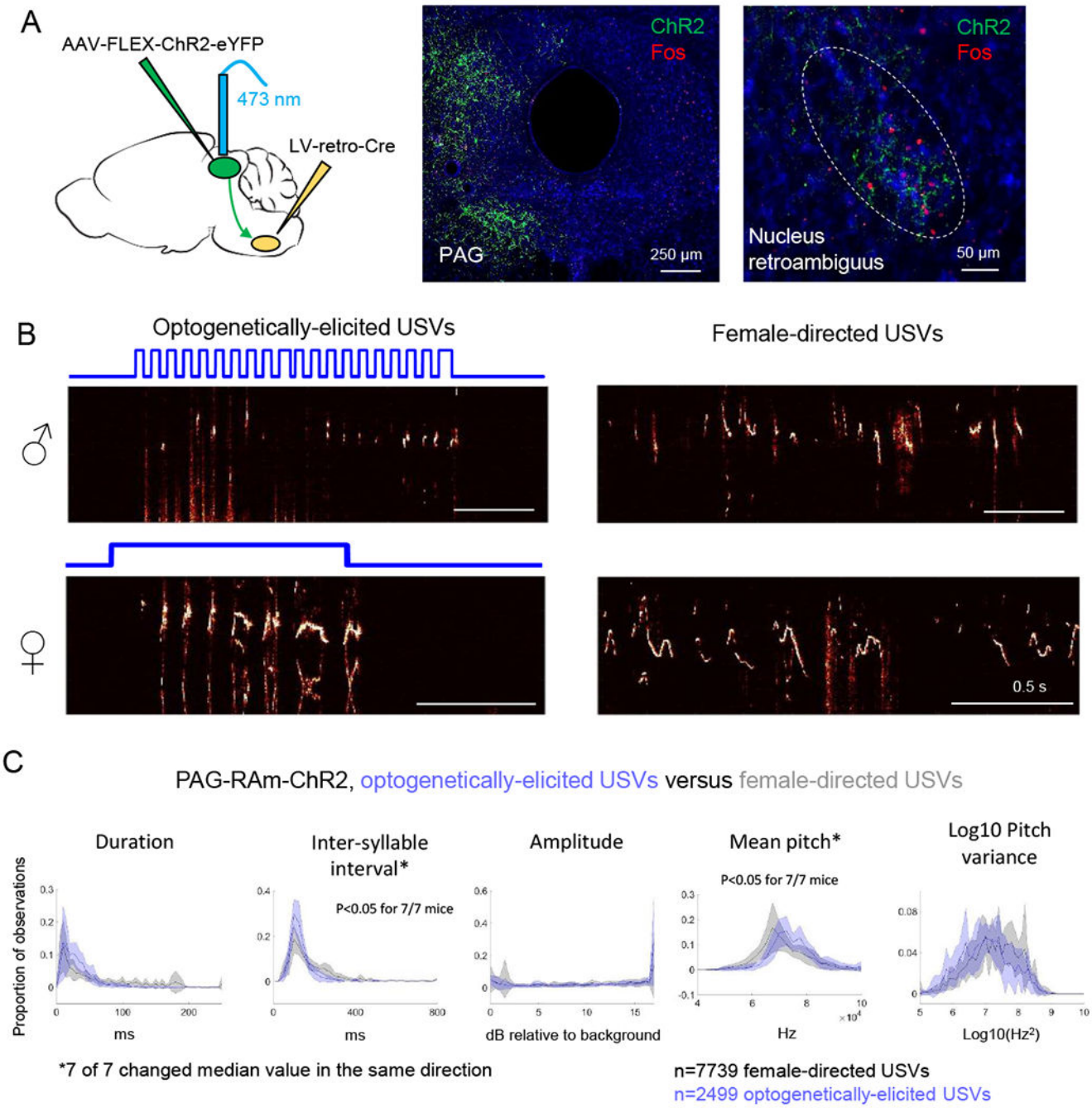

Figure 6. Activating RAm-projecting PAG neurons elicits USVs in male and female mice

(A) (Left) Schematic showing the viral strategy used to express ChR2 in PAG-RAm neurons. Middle and right panels are confocal images of PAG (middle) and RAm (right), showing ChR2 labeling (green) and Fos expression (red) following USV production. (B) Spectrograms comparing USVs elicited by optogenetic activation of PAG-RAm neurons (left) and female-directed USVs (right) from the same animals. Top row shows example spectrograms from a male mouse, and the spectrograms in the bottom row are from a female. (C) Distributions of 5 acoustic parameters are shown for optogenetically-elicited

USVs (blue) and female-directed USVs (gray) for N = 4 male and N = 3 female PAG_{RAm}-ChR2 mice (N = 2 females excluded from analysis that produced few female-directed USVs). Asterisks indicate acoustic parameters whose median value changed significantly in the same direction for 7/7 mice ($p < 0.05$, Mann Whitney U tests.) See also Fig. S2 and S6.

KEY RESOURCES TABLE

REAGENT or RESOURCE	SOURCE	IDENTIFIER
Antibodies		
Goat polyclonal anti-Fos	Santa Cruz	Cat# sc52-g; RRID: AB_2629503
Bovine anti-goat, Alexa Fluor 488 conjugate	Jackson Immuno Research	Cat# 805-545-180; RRID: AB_2340883
Bovine anti-goat, Alexa Fluor 594 conjugate	Jackson Immuno Research	Cat# 805-585-180
Neuro Trace 435/455	Invitrogen/Thermo Fischer Scientific	Cat# N21479
Bacterial and Virus Strains		
AAV2/1-CAG-FLEX-GFP	UNC Vector Core	n/a
AAV2/8-hSyn-FLEX-GFP	UNC Vector Core	n/a
AAV-hSyn-FLEX-hM3Dq-mCherry	Krashes et al., 2011	44361-AAV8; RRID: Addgene_44361
AAV-hSyn-FLEX-hM3Dq-mCherry	UNC Vector Core	n/a
AAV2/1-CBA-FLEX-ChR2-mCherry	Atasoy et al., 2008	18916; RRID: Addgene_18916
AAV2/1-hSyn-ChR2-eYFP	Karl Deisseroth	26973-AAV1; RRID: Addgene_26973
LV-retro-Cre	Nelson et al., 2013	n/a
AAV2/8-hSyn-FLEX-TeLC-P2A-GFP	Zhang et al., 2015	n/a
CANE-LV-Cre	Sakurai et al., 2016	n/a
$EnvA^{M5}$-LV-Cre	Sakurai et al., 2016	n/a
EnvA-LV-Cre	Sakurai et al., 2016	n/a
Chemicals, Peptides, and Recombinant Proteins		
Clozapine N-oxide	Sigma	Cat# C0832
Clozapine N-oxide	Duke Small Molecule Synthesis Facility	n/a
Experimental Models: Organisms/Strains		
Fos TVA	Jackson Labs	Stock 027831
Vglut2-ires-Cre	Jackson Labs	Stock 028863
PV-Cre	Jackson Labs	Stock 008069
Software and Algorithms		
MATLAB	Mathworks	http://mathworks.com, RRID:SCR_001622
ImageJ	NIH	http://imagej.nih.gov/ij, RRID:SCR_003070
ZEN	Zeiss	http://zeiss.com
Spike7	CED	ced.co.uk